Received September 4, 2019, accepted September 17, 2019, date of publication September 23, 2019,
date of current version October 7, 2019.

Digital Object Identifier 10.1109/ACCESS.2019.2943181

Thermoelectric Parameter Modeling of Single-Layer Graphene Considering Carrier Concentration and Mobility With Temperature and Gate Voltage

NING WANG, CONG MENG, ZHI-HAO MA, CONG GAO, HONG-ZHI JIA, GUO-RONG SUI, AND XIU-MIN GAO
Shanghai Key Laboratory of Modern System, Engineering Research Center of Optical Instrument and System, Ministry of Education, University of Shanghai for Science and Technology, Shanghai 200093, China

Corresponding author: Xiu-Min Gao (xiumin_gao@aliyun.com)

This work was supported in part by the National Key Research and Development Plan-Earth Observation and Navigation Key Special Project under Grant 2017YFB0503102, in part by the National Key Research and Development Program of China under Grant 2018YFC1313803, and in part by NSFC under Grant 61804096.

ABSTRACT Single-layer graphene (SLG) sheets can exhibit thermoelectric properties under the control of gate voltage. The controlled factors and regulation mechanism of SLG thermoelectric properties have become research hotspots. In this paper, a SLG thermoelectric parameter model considering carrier concentration and mobility with temperature and gate voltage is proposed. Based on the proposed model, the square resistance (R_s) and Seebeck coefficient (S) of the SLG are calculated. The results show that the maximum value of R_s decreases from 5.8 KΩ to 3.2 KΩ at the Dirac voltage when the temperature increases from 100 K to 500 K. A large and stable S can be obtained at high voltages and temperatures. The maximum value of S can reach 161.3 μV/K at $T = 500$ K, exhibiting a more obvious thermoelectric characteristic. Simultaneously, the saturation law of the power factor (Q) with the change of gate voltage and the amplitude regulation of Q by temperature are obtained. This work can provide a theoretical basis for analyzing the thermoelectric characteristics of SLG.

INDEX TERMS Graphene, seebeck coefficient, square resistance, thermoelectric effect.

I. INTRODUCTION

The thermoelectric effect is the direct conversion of heat into electricity or electricity into heat and includes the Seebeck effect, the Peltier effect and the Thomson effect [1]. As a carrier of the thermoelectric effect, the thermoelectric material realizes the mutual transformation between electricity and heat [2]. Recently, with the emergence of new thermoelectric materials [3], low-dimensional thermoelectric materials exhibit excellent electrical and thermal characteristics and have attracted attention from researchers. Graphene is one of these new low-dimensional thermoelectric materials.

Graphene, a new two-dimensional thin film material composed of carbon atoms, has a thickness of only one carbon atom (0.34 nm). Since it was first discovered in 2004 [4], graphene has become the most attractive nanomaterial due to its excellent electrical, thermal and optical properties [5]–[9]. Initially, research on graphene materials was not carried out in the field of thermoelectrics but focused on light, heat and electricity. For example, a research team from Nankai University confirmed that graphene exhibits strong polarization-dependent optical absorption under total internal reflection [10], that is, graphene can be used as a sensitive material for fiber-optic sensors, which makes it possible to replace the precious metal layer in fiber sensors with a graphene layer [11]. In addition, the thermal conductivity of SLG has been measured up to 5300 W/mK by using Raman spectroscopy [12]. This property makes graphene an excellent material for thermal management and provides additional power for the integration of CMOS devices and circuits. In the temperature environment of 5 K, the electron mobility in SLG is captured up to 200,000 cm^2/Vs [13]. Hence, it can be used as a high-speed conduction channel in signal transmission. In addition to the above fields, the research and application

The associate editor coordinating the review of this manuscript and approving it for publication was F. R. Islam.

This work is licensed under a Creative Commons Attribution 4.0 License. For more information, see http://creativecommons.org/licenses/by/4.0/

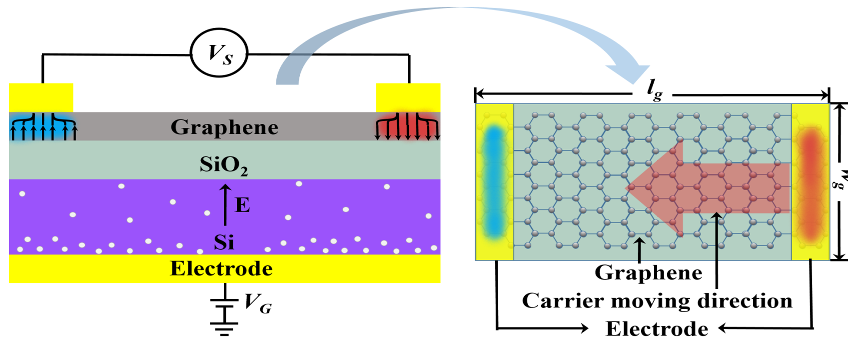

FIGURE 1. Schematic diagram of the Single-layer graphene system structure. A graphene nanoribbon was deposited on silicon dioxide with a thickness of 300 nm, and silicon was used as a substrate.

of graphene as a thermoelectric material are being explored gradually. However, early research on the ability of graphene to play a role in thermoelectric energy conversion is not optimistic. Experiments by Michael S. Fuhrer et al. show that temperature has a limited effect on electron mobility in graphene [14]. Its Seebeck coefficient is very low due to the zero band gap of ideal graphene [15], which makes graphene unsuitable as a thermoelectric material. It was not until 2007 that this streak was broken by Melinda Y. Han. Han found that the electron band gap of graphene is inversely proportional to the width of graphene sheets [16]. That is, the gap of graphene has physical regulation characteristics. Therefore, graphene nanoribbons with open electron gaps can be obtained by changing the width of the graphene [17], [18]. Experiments have confirmed that the carrier mobility of graphene changes with the generation of its band gap [19]. However, this scale regulation is difficult to use flexibly after fabrication. K. S. Novoselov's team found that graphene exhibited a bipolar electrical tuning effect when an external bias voltage was applied. A large number of electrons (holes) are induced by the positive (negative) gate voltage, and all of the induced carriers are movable [20], which lays the foundation for regulating the graphene semiconductor characteristics through voltage. Conversely, the carrier mobility of single-layer, double-layer and triple-layer graphene and their temperature dependence were systematically studied by Zhu's team [21]. The mobility of SLG increases with the increase of temperature and carrier density. Using silicon dioxide (SiO_2) as the substrate, Dorgan *et al.* [22] obtained changes in the SLG carrier mobility and saturation velocity with temperature. Ouyang *et al.* [23] solved the atomic electron and phonon transport in the form of the non-equilibrium Green's function, which caused the Seebeck coefficient to be large. At a temperature of 300 K, S is calculated to be a maximum of 90 μV/K [24]. It can be seen that in addition to voltage, temperature can be used as an additional control means to regulate the carrier and thermoelectric parameters of graphene.

The studies mentioned above provide a theoretical basis for exploring the electrical and thermoelectric properties of graphene. The carrier concentration and mobility of SLG, including the thermoelectric parameters, are regulated by the temperature and gate voltage. In this paper, a model of the SLG thermoelectric parameters that considers the carrier concentration and mobility at various temperatures and gate voltages is proposed. The regulation of R_s by different gate voltages and temperatures is discussed. The thermoelectric parameters S, Q and V_S of SLG are calculated, and the adjustment law of the gate voltages and temperatures on these parameters is explored.

II. ELECTRICAL CHARACTERISTICS FOR SLG

Fig. 1 shows the device structure of SLG in its operating state. In this structure, SiO_2 is used as the intermediate oxide layer, and a highly doped silicon substrate is used as the back gate. The carrier concentration in the SLG can be regulated by the vertical electric field applied by the back gate voltage (V_G). V_S is the Seebeck voltage. A potential difference will be produced between two dissimilar electrical conductors or semiconductors if there is a temperature gradient across them [25], and this voltage difference is called the Seebeck voltage. $l_g = 7\ \mu$m, $w_g = 4\mu$m are the length and width of the graphene nanoribbon, respectively. In this section, the variations of the carrier concentration and the mobility in the SLG are studied, and the square resistance of the SLG is calculated to investigate the electrical properties of SLG under an electric field.

A. CARRIER CONCENTRATION

The relationship between the gate voltage and the carrier concentration (n_g) induced by the gate voltage can be obtained from [21]

$$n_g = (V_G - V_0) \,/ \left(q \left(\frac{1}{C_{ox}} + \frac{1}{C_q} \right) \right) \tag{1}$$

where $C_{ox} = \varepsilon_0 \varepsilon_r / t_{ox}$ is the oxide capacitance, ε_0, ε_r and t_{ox} are the vacuum dielectric constant, the relative dielectric constant and the thickness of SiO_2, respectively. C_q is the quantum capacitance of graphene, and q is the electron charge. For SiO_2 with a thickness of 300 nm, C_q in (1)

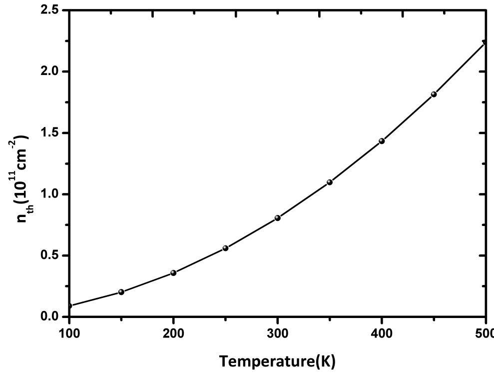

FIGURE 2. The change in thermal carrier density induced by temperature.

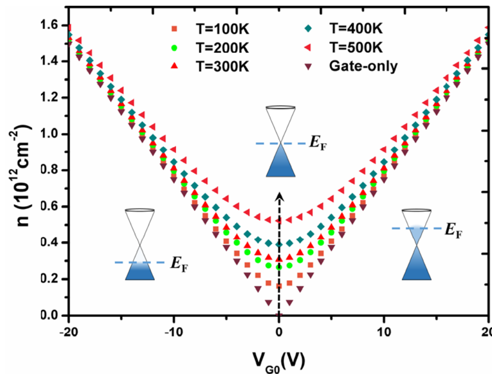

FIGURE 3. The total carrier concentration n of SLG as a function of V_{G0} at different temperatures, the Gate-only curve represents the functional relationship between ng and V_{G0} without regarding to temperature.

can be ignored if the carrier concentration is greater than $2\times10^{11}\text{cm}^{-2}$, where $C_{ox} << C_q$. V_G refers to the back gate voltage, and V_0 is the Dirac voltage. For an ideal SLG, the Fermi level is at the Dirac point ($V_0 = 0$ V), that is, the concentrations of electrons and holes at this point are equal. However, $V_0 \neq 0$ V, which is the result of the deviation of the Dirac point caused by impurities, defects and other factors. In this paper, $V_{G0} = V_G$-V_0. Taking the influence of the minimum carrier density $n_0 = ((n^*/2)^2 + n_{th}^2)^{1/2}$ into account, the total carrier concentration in graphene can be expressed as

$$n = \sqrt{\left(\frac{C_{ox}V_{G0}}{q}\right)^2 + 4\left(\left(\frac{n^*}{2}\right)^2 + n_{th}^2\right)} \tag{2}$$

where n^* is the residual carrier puddle density, and n_{th} is the thermal carrier density. $n_{th} = (\pi/6)(K_BT/\hbar v_F)^2$, where v_F and $\hbar$ are the Fermi velocity and the reduced Planck constant, respectively. n contains n_{th} and n_g. The line in Fig. 2 indicates that T has a positive effect on n_{th}. In Fig. 3, the dependence of n on T and V_{G0} is depicted. When $V_{G0} < 0$ V, the Fermi level of SLG is in the valence band. As V_{G0} approaches 0 V, the Fermi level moves from the valence band to the Dirac point. At the Dirac point ($V_{G0} = 0$ V), the carrier concentration in the SLG channel is the lowest. When $V_{G0} > 0$ V, the Fermi level enters the conduction band, and the carrier concentration in the SLG channel also begins to rise. At the same reference temperature, the larger the absolute value of V_{G0}, the higher the n. The Gate-only curve denotes the relationship between n_g and V_{G0}. n_g is close to zero at V_{G0} ~0 V, but T has a positive effect on n_{th}. In the case of $V_{G0} = 2$ V where $n_g = 0.15\times10^{12}\text{cm}^{-2}$, n=$0.16\times10^{12}$ cm^{-2} at $T = 100$ K, whereas n can reach $0.52\times10^{12}\text{cm}^{-2}$ at $T = 500$ K. n has risen more than three times under the regulation of T. However, $n_g = 1.5\times10^{12}\text{cm}^{-2}$ when $V_{G0} = 20$ V. Meanwhile, n=$1.51\times10^{12}\text{cm}^{-2}$ at $T = 100$ K, and n=$1.59\times10^{12}\text{cm}^{-2}$ at $T = 500$ K. Thus, in the low gate voltage range, n_{th} plays a leading role on n. Whereas the carrier concentration curves at different temperatures gradually coincide with the Gate-only curve with the increase of V_{G0}, indicating that n_g begins to dominate. This suggests that n is subject to different main control mechanisms under different conditions, and this result is consistent with reference [22]. The desired carrier concentration can be achieved by equalizing T and V_{G0}.

B. CARRIER MOBILITY

The carrier mobility (μ) refers to the overall speed of electrons and holes in the semiconductor. To simplify the calculation, both μ and n_0 have been used as constant values for subsequent calculations in many studies [26], [27]. In fact, μ will also change as the conditions imposed by the system change [28].

$$\mu = \frac{\mu_0}{1 + \left(\sqrt{\left(\frac{C_{ox}(V_{G0})}{q}\right)^2 + 4\left(\left(\frac{n^*}{2}\right)^2 + n_{th}^2\right)}/n_{ref}\right)^{\alpha}} \times \frac{1}{1 + \left({}^{T}/_{T_{ref}} - 1\right)^{\beta}} \tag{3}$$

where μ_0 is the low field mobility, T_{ref} and n_{ref} are the reference temperature and the reference charge density [29], respectively, and α and β are constants with values of 2.2 and 3, respectively. The values of T_{ref}, n_{ref}, α and β are derived from the traditional model, and we take them from [22], [29]. In (3), μ is negatively correlated with T and V_{G0}.

In Fig. 4, the value of μ is plotted as V_{G0} and T vary. The peak value of μ is 6610 cm^2/Vs at $T = 100$ K, which is smaller than the carrier mobility in pure graphene sheets. Since the scattering effect of the carrier by the optical phonon in the SiO_2 film is much larger than the one by the SLG itself, a large drop in μ occurs, and n of the SLG is enhanced.

A high T and a large V_{G0} lead to a decrease in μ, which is consistent with [22]. Based on the work in [21], when the temperature is low, such as $T = 100$ K, μ is mainly limited by Coulomb scattering and short-range scattering. Coulomb scattering is independent of the carrier concentration, whereas short-range scattering is proportional to the carrier concentration. Therefore, for the curve of $T = 100$ K, Coulomb scattering is enhanced when V_{G0} is adjusted to increase the carrier concentration, and μ is decreased. μ drops

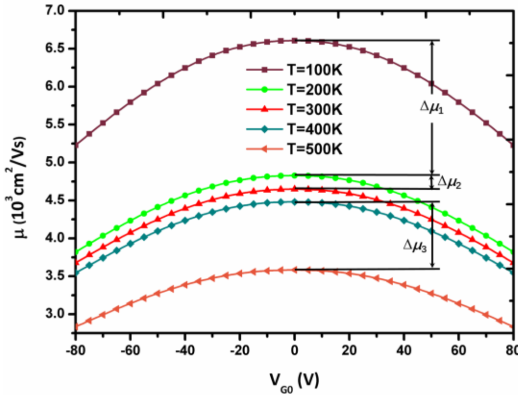

FIGURE 4. Carrier mobility as a function of V_{G0} at different temperatures.

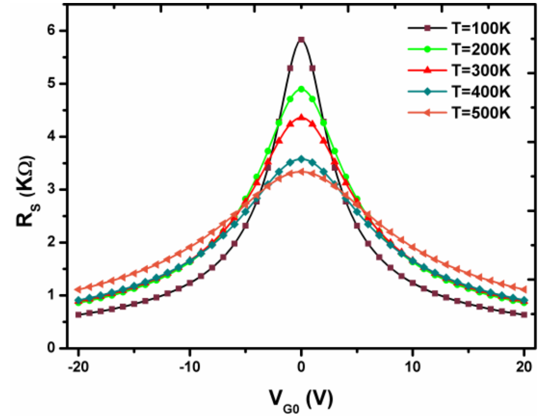

FIGURE 5. R_s as a function of V_{G0} at different temperatures.

rapidly by $\Delta\mu_1 = 1783$ cm2/Vs when the temperature is raised from 100 K to 200 K because the increase in temperature promotes the acoustic phonon scattering of SLG. The magnitude of acoustic phonon scattering is much larger than that of Coulomb scattering and short-range scattering, which leads to a larger decrease in μ. μ decreases slightly when $T = 200$ K, 300 K, or 400 K, with $\Delta\mu_2 = 177$ cm2/Vs, which is related to $T_{\mathrm{ref}} = 300$ K and $\beta = 3$. The change in the second half of (3) can be ignored if the difference between T and T_{ref} is small, which results in a smaller change in μ. However, μ drops sharply by $\Delta\mu_3 = 898$ cm^2/Vs as T continues to rise from 400K to 500 K. Since the acoustic phonon scattering of SLG is proportional to T and the scattering of surface polar phonons on the SiO_2 substrate is excited by high temperatures, μ is further attenuated.

C. SQUARE RESISTANCE

The formula for calculating the square resistance, $R_s = 1/q\mu n$, was established according to the model proposed by Grosse *et al.* [30]. However, this expression simplifies the carrier concentration and mobility. Based on the above results, both n and μ are affected by T and V_{G0}. Combined with (2), the expression of Rs can be written as

$$R_s = \frac{\left(1 + \left(n/n_{ref}\right)^{\alpha}\right)\left(1 + \left(T/T_{ref} - 1\right)^{\beta}\right)}{-q\mu_0 n} \quad (4)$$

To introduce the two variables T and V_{G0}, n_{th} is used in (3), and R_s can be obtained by combining (3) and (4):

$$R_s = \frac{1 + \left(\sqrt{\left(\frac{C_{ox}(V_{G0})}{q}\right)^2 + 4\left(\left(\frac{n^*}{2}\right)^2 + \left(\frac{\pi}{6}\left(\frac{K_B T}{\hbar v_F}\right)^2\right)^2\right)} / n_{ref}\right)^{\alpha}}{-q\mu_0 \sqrt{\left(\frac{C_{ox}(V_{G0})}{q}\right)^2 + 4\left(\left(\left(\frac{n^*}{2}\right)^2 + \left(\frac{\pi}{6}\left(\frac{K_B T}{\hbar v_F}\right)^2\right)^2\right)\right)}} \times \left(1 + \left(T/T_{ref} - 1\right)^{\beta}\right) \quad (5)$$

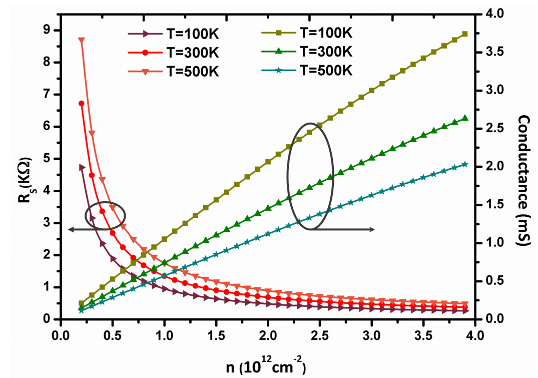

FIGURE 6. R_s (left) and conductance (right) as a function of n at different temperatures.

In (5), once the material used is given, many parameters in the formula are also determined. As a result, R_s is only controlled by the two variables T and V_{G0}. Fig. 5 depicts the relationship of R_s and V_{G0} at different temperatures. R_s is greatly affected by T at low V_{G0} due to the dominant position of n_{th}. Moreover, the value of R_s at different temperatures reaches the maximum at $V_{G0} = 0$ V. n is the smallest at this point, and R_s is inversely proportional to n. Note that the peak value of R_s can reach 5.3 KΩ at $T = 100$ K, whereas the peak value is only 3.3 KΩ at $T = 500$ K. From these results, the effect of T on R_s cannot be ignored when V_{G0} is in a low range. However, the dominant position is occupied by n_g as V_{G0} rises gradually, which means that R_s begins to be regulated by V_{G0}. With the increase of T, the lattice vibration is strengthened, and the phonon motion is intensified, resulting in an increase in scattering. Therefore, in the case of a large V_{G0}, a higher T corresponds to a larger R_s.

Since conductance is inversely proportional to R_s, Fig. 6 can be obtained by combining with (4). Fig. 6 shows the relationship of R_s and conductance as a function of n at different temperature conditions. R_s rises sharply when n is less than 0.5×10^{12}cm^{-2}, and therefore, SLG is not suitable for use as a thermoelectric device if the internal

carrier concentration is too small. As n becomes larger, the effect of T on R_s gradually weakens, whereas the impact on conductance begins to be apparent. The conductance and n are approximately linearly related, contrary to the relationship between R_s and n. Similarly, high T values exacerbate the scattering of acoustic phonons and surface polar phonons on the SiO_2 substrate, reducing μ. The conductance is proportional to μ, and thus, the conductance is reduced as T increases. The conductance can be altered by adjusting the internal carrier concentration of SLG, and the carrier concentration can be regulated by modifying the gate voltage, which provides a more convenient form for the conductivity revision of SLG. The purpose of increasing the conductance of SLG can also be achieved by adjusting the T of μ and n.

III. HERMOELECTRIC CHARACTERISTICS OF SLG

The Seebeck effect, also known as the first thermoelectric effect, is a thermoelectric phenomenon in which V_S is produced. However, the performance of a thermoelectric material is not usually determined by V_S; rather, it is determined by the thermoelectric figure of merit ZT [31].

$$ZT = \frac{S^2 \sigma T}{K} \tag{6}$$

where S and K are the Seebeck coefficient and the thermal conductivity, respectively. $\sigma = l_g/(R_s w_g d)$ is the conductivity, and d is the thickness of the SLG. Generally, the larger the ZT value, the better the thermoelectric properties of the material. It can be seen from (6) that it is necessary to increase S and σ or to weaken K to improve the performance of SLG.

A. SEEBECK COEFFICIENT

According to the Mott relationship [32]–[34], the expression of S can be obtained as follows:

$$S = -\frac{\pi^2 K_b^2 T}{3q} \frac{1}{G} \frac{dG}{dE} = \frac{\pi^2 K_b^2 T}{3q} \frac{1}{R} \frac{dR}{dE} \tag{7}$$

where K_B and $E = E_F$ are the Boltzmann constant and the Fermi level, respectively. The dependence of E_F on the carrier density can be acquired from the tight binding calculation [35]. For SLG, $E_F = \hbar v_F (\pi n)^{1/2}$. To obtain the influence of the gate voltage on S, the term $(1/R)(dR/dE)$ is replaced by $(1/R)(dR/dV_G)(dV_G/dE)$ in the calculation. Solving dR/dV_G and dV_G/dE and bringing the result into (7) yields

$$S = \frac{-2\pi^{\frac{3}{2}} K_B^2 T \left(\frac{C_{ox}(V_{G0})}{q}\right) \sqrt{\left|\frac{C_{ox}(V_{G0})}{q}\right|}}{3q\hbar v_F \left(\left(\frac{C_{ox}(V_{G0})}{q}\right)^2 + 4\left(\left(\frac{n^*}{2}\right)^2 + \frac{\pi}{6}\left(\frac{K_B T}{\hbar v_F}\right)^2\right)\right)} \tag{8}$$

It is obvious that S is controlled by V_{G0} and T in (8). The sign of S is related to the type of carrier. Thus, the carriers induced in the channel are electrons when a positive gate voltage is applied and S is negative. Conversely, S is positive when the carriers in the channel are holes. Fig. 7 shows the variation of S with V_{G0} for different temperatures. At $V_{G0} = 0$ V, when E_F is at the charge neutral point, SLG is more

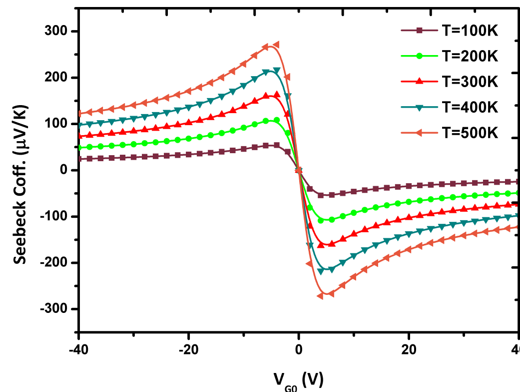

FIGURE 7. The variation of the Seebeck coefficient with V_{G0} for different temperatures.

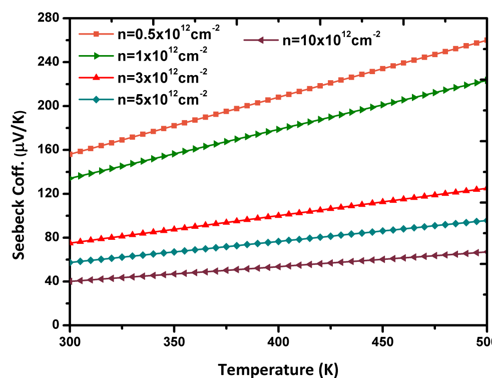

FIGURE 8. The Seebeck coefficient as a function of T at different carrier concentrations.

similar to a conductor. As the carrier density is adjusted by the gate voltage, the E_F of SLG is far away from the charge neutral point as V_{G0} increases. S increases significantly with V_{G0} within the low voltage range and then begins to drop slightly in the high voltage range, presenting the expected thermoelectric properties. This phenomenon is consistent with the results in [32]. Moreover, T has a positive correlation with the absolute value of S. High T values correspond to high $|S|$.

When the majority carrier is a hole, that is, when V_{G0} is negative, S has a positive value. Fig. 8 shows the Seebeck coefficient as a function of T at different hole carrier concentrations. In Fig.8, the sensitivity of S to T at low carrier concentrations is stronger than that at high carrier concentrations because a high gate voltage leads to a high n_g and then acts on S. The higher the gate voltage, the larger the n_g, and the weaker the regulation of n_{th} on S caused by T. For the curve of $n = 0.5\times10^{12}$ cm^{-2} where $V_{G0} = -5$ V, $S = 156.05$ μV/K at $T = 300$ K, and $S = 208.07$ μV/K at $T = 400$ K, whereas S can reach 260.08 μV/K at $T = 500$ K. It can be seen that the elevated temperature can significantly increase S at low V_{G0} values. In addition, taking $T = 300$ K as an example, $S = 134.06$ μV/K when $n = 1\times10^{12}$cm^{-2} and $V_{G0} = -13$ V, and $S = 75.06\mu$V/K when $n = 3\times10^{12}$ cm^{-2}

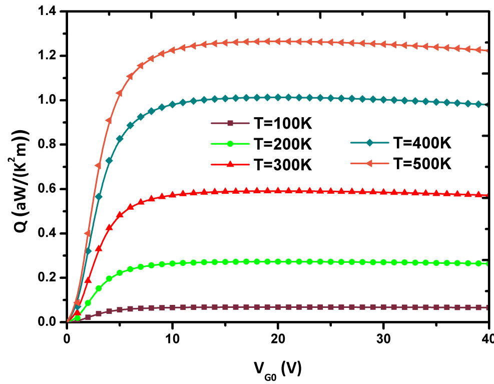

FIGURE 9. Q as a function of V_{G0} at different temperatures.

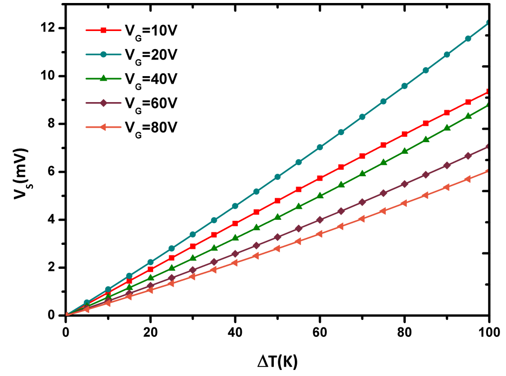

FIGURE 10. V_S as a function of ΔT at different gate voltages.

and $V_{G0} = -40$ V. Further, $S = 57.39$ μV/K when $n = 5\times10^{12}$ cm^{-2} and V_{G0} reaches -67 V. It can be seen that the value of S continues to decrease with the increase of V_{G0}. In summary, the regulation of S by appropriate voltage and temperature values is essential to improve the thermoelectric characteristics of SLG.

B. POWER FACTOR

The power factor ($Q = S^2\sigma$) of SLG is also calculated in this paper. As shown in Fig. 9, Q increases first with V_{G0} and then becomes saturated, indicating that an excessively high gate voltage is not useful for improving Q. Q begins to stabilize when V_{G0} >5 V at $T = 100$K. However, Q tends to stabilize when V_{G0} >14 V at $T = 500$. Therefore, the reasonable working range of V_{G0} should be controlled in the range of 5∼14V. In addition, T has a benefit on the improvement of Q. However, different semiconductor devices have different production processes, thus their operating temperatures cannot be precisely controlled. For example, given that the operating temperature of a typical device is approximately 300∼400 K, it is more convenient to adjust V_{G0} to obtain a higher Q. Therefore, appropriate conditions should be selected to obtain the desired results when controlling the thermoelectric properties of graphene.

C. SEEBECK VOLTAGE

Based on the definition of the Seebeck effect, V_S is produced when there is a temperature difference between the two ends in the system. One end is controlled to the reference temperature (T_L), the other end is the high temperature state (T_H), and T_H is set as the variable. $\Delta T = T_H$ - T_L. Based on the analysis of the Seebeck coefficient above and the influence of temperature changes on each parameter, the expression of V_S can be written as [36]

$$V_s = -\frac{\pi^{\frac{3}{2}} K_B^2 (T_H + T_L) \left(\frac{C_{ox}(V_G - V_0)}{q}\right) \sqrt{\left|\frac{C_{ox}(V_G - V_0)}{q}\right|}}{3q\hbar v_F \left(\frac{C_{ox}(V_G - V_0)}{q}^2 + 4\left(\left(\frac{n^*}{2}\right)^2 + \frac{\pi}{6}\left(\frac{K_B T}{\hbar v_F}\right)^2\right)\right)} \times (T_H - T_L) \quad (9)$$

In Fig. 10, when the temperature difference between the two ends of the SLG is not obvious, V_S is small. However, with the augmentation of ΔT, the increasing velocity of V_S is slightly promoted. Since V_S is proportional to the Seebeck coefficient, the energy of the carrier in the hot end becomes stronger due to a high T_H value, leading to an increase of the difference between the Fermi levels at both ends of the SLG and enhancing the Seebeck effect. In addition, the $V_G = 10$ V curve indicates that a low gate voltage is not beneficial to the generation of V_S. In the case of $V_G = 20$ V and $\Delta T = 100$ K, the value of n is approximately 1.1×10^{12} cm^{-2}, and V_S can reach 12.3 mV. This result is consistent with the results in [35]. With the continued rise of V_G, V_S is in a falling state. From the previous analysis, it can be seen that S first increases and then decreases with the increase of V_{G0}, and the variation law of V_S with the gate voltage is consistent with that of S with the gate voltage. It can be seen that when SLG is used for energy harvesting, the appropriate gate voltage helps to increase the obtained V_S value.

IV. CONCLUSION

In this paper, the influences of T and V_{G0} on the carrier concentration and mobility of SLG are analyzed. The carrier concentration, mobility and the thermoelectric parameters of SLG are combined through the two variables T and V_{G0}. The square resistance, the Seebeck coefficient, the power factor and the Seebeck voltage of SLG are calculated, and the mechanism of these thermoelectric parameters under different conditions is analyzed in detail. The results show that T and V_{G0} play different roles in the thermoelectric parameters of SLG at different stages. In addition, the thermoelectric properties of SLG can be regulated by controlling V_{G0} and T. The power factor of SLG can also be improved by applying an appropriate gate voltage and temperature. This paper provides a theoretical analysis for a better understanding of the variation characteristics and adjustability of the thermoelectric parameters of SLG.

REFERENCES

[1] K.-I. Uchida, H. Adachi, T. Kikkawa, A. Kirihara, M. Ishida, S. Yorozu, S. Maekawa, and E. Saitoh, "Thermoelectric generation based on spin seebeck effects," *Proc. IEEE*, vol. 104, no. 10, pp. 1946–1973, Oct. 2016.

[2] K.-S. Yoon, S.-W. Hong, and G.-H. Cho, "Double pile-up resonance energy harvesting circuit for piezoelectric and thermoelectric materials," *IEEE J. Solid-State Circuits*, vol. 53, no. 4, pp. 1049–1060, Apr. 2018.

[3] D. Kim, J. Kally, N. Samarth, and S. Tadigadapa, "Microfabricated testbench for high throughput measurement of thermal and thermoelectric properties of low-dimensional materials," *J. Microelectromech. Syst.*, vol. 26, no. 2, pp. 396–405, Apr. 2017.

[4] A. K. Geim and K. S. Novoselov, "The rise of graphene," *Nature Mater.*, vol. 6, no. 3, pp. 183–191, Mar. 2007.

[5] N. M. R. Peres, J. M. B. L. dos Santos, and T. Stauber, "Phenomenological study of the electronic transport coefficients of graphene," *Phys. Rev. B, Condens. Matter*, vol. 76, no. 7, Aug. 2007, Art. no. 073412.

[6] S. D. Sarma, S. Adam, E. H. Hwang, and E. Rossi, "Electronic transport in two-dimensional graphene," *Rev. Mod. Phys.*, vol. 83, no. 2, pp. 407–470, 2011.

[7] T. Stauber, N. M. R. Peres, and F. Guinea, "Electronic transport in graphene: A semiclassical approach including midgap states," *Phys. Rev. B, Condens. Matter*, vol. 76, Nov. 2007, Art. no. 205423.

[8] N. Wang, H.-W. Li, C. Ding, L.-Y. Shi, H.-Z. Jia, Z.-D. Ren, and Z.-Y. Zhao, "A double-voltage-controlled effective thermal conductivity model of graphene for thermoelectric cooling," *IEEE Trans. Electron Devices*, vol. 65, no. 3, pp. 1185–1191, Mar. 2018.

[9] T. Löfwander and M. Fogelström, "Impurity scattering and Mott's formula in graphene," *Phys. Rev. B, Condens. Matter*, vol. 76, no. 19, Nov. 2007, Art. no. 193401.

[10] Q. Ye, J. Wang, Z. Liu, Z.-C. Deng, X.-T. Kong, F. Xing, X.-D. Chen, W.-Y. Zhou, C.-P. Zhang, and J.-G. Tian, "Polarization-dependent optical absorption of graphene under total internal reflection," *Appl. Phys. Lett.*, vol. 102, no. 2, Jan. 2013, Art. no. 021912.

[11] Y. Chung, W. Jin, B. Lee, J. Canning, K. Nakamura, and L. Yuan, "25th international conference on optical fiber sensors," *Proc. SPIE*, vol. 10323, Apr. 2017, Art. no. 103237R.

[12] A. A. Balandin, S. Ghosh, W. Bao, I. Calizo, D. Teweldebrhan, F. Miao, and C. N. Lau, "Superior thermal conductivity of single-layer graphene," *Nano Lett.*, vol. 8, no. 3, pp. 902–907, 2008.

[13] K. I. Bolotin, K. J. Sikes, Z. Jiang, M. Klima, G. Fudenberg, J. Hone, P. Kim, and H. L. Stormer, "Ultrahigh electron mobility in suspended graphene," *Solid State Commun.*, vol. 146, pp. 351–355, Jun. 2008.

[14] F. R. Service, "Carbon sheets an atom thick give rise to graphene dreams," *Science*, vol. 324, no. 5929, pp. 875–877, May 2009.

[15] J. H. Seol, I. Jo, A. L. Moore, L. Lindsay, Z. H. Aitken, M. T. Pettes, X. Li, Z. Yao, R. Huang, D. Broido, N. Mingo, R. S. Ruoff, and L. Shi, "Two-dimensional phonon transport in supported graphene," *Scinece*, vol. 328, no. 5975, pp. 213–216, Apr. 2010.

[16] M. Y. Han, B. Özyilmaz, Y. Zhang, and P. Kim, "Energy band-gap engineering of graphene nanoribbons," *Phys. Rev. Lett.*, vol. 98, no. 20, May 2007, Art. no. 206805.

[17] A. Zhang, H. F. Teoh, Z. Dai, Y. P. Feng, and C. Zhang, "Band gap engineering in graphene and hexagonal BN antidot lattices: A first principles study," *Appl. Phys. Lett.*, vol. 98, no. 2, Jan. 2011, Art. no. 023105.

[18] A. Hassan, M. Hossain, S. A. Sobhan, M. R. Haq, and T. A. Siddiquee, "Armchair graphene nanoribbon photonics," in *Proc. Sci. Inf. Conf.*, Jul. 2015, pp. 1108–1112.

[19] L. Yang, C.-H. Park, Y.-W. Son, M. L. Cohen, and S. G. Louie, "Quasiparticle energies and band gaps in graphene nanoribbons," *Phys. Rev. Lett.*, vol. 99, no. 18, Nov. 2007, Art. no. 186801.

[20] K. S. Novoselov, A. K. Geim, S. V. Morozov, D. Jiang, M. I. Katsnelson, I. V. Grigorieva, S. V. Dubonos, and A. A. Firsov, "Two-dimensional gas of massless dirac fermions in graphene," *Nature*, vol. 438, no. 7065, pp. 197–200, Nov. 2005.

[21] W. Zhu, "Carrier scattering, mobilities and electrostatic potential in mono-, bi- and tri-layer graphenes," 2009, *arXiv:0908.0749*. [Online]. Available: https://arxiv.org/abs/0908.0749

[22] V. E. Dorgan, M.-H. Bae, and E. Pop, "Mobility and saturation velocity in graphene on SiO_2," *Appl. Phys. Lett.*, vol. 97, no. 8, Aug. 2010, Art. no. 082112.

[23] Y. Ouyang and J. Guo, "A theoretical study on thermoelectric properties of graphene nanoribbons," *Appl. Phys. Lett.*, vol. 94, no. 26, 2009, Art. no. 263107.

[24] X.-Z. Yan, Y. Romiah, and C. S. Ting, "Thermoelectric power of Dirac fermions in graphene," *Phys. Rev. B, Condens. Matter*, vol. 80, no. 16, Oct. 2009, Art. no. 165423.

[25] J.-S. Park and C.-S. Huh, "A study on improved efficiency and cooling LED lighting using a seebeck effect," in *Proc. Int. Conf. Power Eng. Renew. Energy*, Jul. 2012, pp. 1–3.

[26] A. Amirhosseini and R. Safian, "Photo-thermoelectric current enhancement in graphene-based photodetectors using plasmonic nanostructures," *IEEE J. Sel. Topics Quantum Electron.*, vol. 24, no. 2, Mar./Apr. 2018, Art. no. 4600207.

[27] K. Tsukagoshi, H. Miyazaki, S.-L. Li, A. Kanda, and S. Nakaharai, "Gate-tunable control in graphene semiconductive channel," in *Proc. Int. Workshop Active-Matrix Flatpanel Displays Devices*, Jul. 2012, pp. 305–308.

[28] R. Verma, S. Bhattacharya, and S. Mahapatra, "Modeling of temperature and field-dependent electron mobility in a single-layer graphene sheet," *IEEE Trans. Electron Devices*, vol. 60, no. 8, pp. 2695–2698, Aug. 2013.

[29] N. D. Arora and G. S. Gildenblat, "A semi-empirical model of the MOSFET inversion layer mobility for low-temperature operation," *IEEE Trans. Electron Devices*, vol. 34, no. 1, pp. 89–93, Jan. 1987.

[30] K. L. Grosse, M.-H. Bae, F. Lian, E. Pop, and W. P. King, "Nanoscale Joule heating, peltier cooling and current crowding at graphene–metal contacts," *Nature Nanotechnol.*, vol. 6, no. 5, pp. 287–290, Apr. 2011.

[31] P. Dollfus, V. H. Nguyen, V. T. Tran, M. C. Nguyen, A. Bournel, and J. Saint-Martin, "Thermoelectric effects in graphene and graphene-based nanostructures using atomistic simulation," in *Proc. Int. Workshop Power Timing Modeling*, Sep. 2016, pp. 38–43.

[32] A. Brenneis, F. Schade, S. Drieschner, F. Heimbach, H. Karl, J. A. Garrido, and A. W. Holleitner, "THz-circuits driven by photo-thermoelectric, gate-tunable graphene-junctions," *Sci. Rep.*, vol. 6, Oct. 2016, Art. no. 35654.

[33] Y. M. Zuev, W. Chang, and P. Kim, "Thermoelectric and magnetothermoelectric transport measurements of graphene," *Phys. Rev. Lett.*, vol. 102, no. 9, Mar. 2009, Art. no. 096807.

[34] J. C. W. Song, M. S. Rudner, C. M. Marcus, and L. S. Levitov, "Hot carrier transport and photocurrent response in graphene," *Nano Lett.*, vol. 11, no. 11, pp. 4688–4692, Sep. 2011.

[35] T. J. Echtermeyer, S. Milana, U. Sassi, A. Eiden, M. Wu, E. Lidorikis, and A. C. Ferrari, "Surface plasmon polariton graphene photodetectors," *Nano Lett.*, vol. 16, no. 1, pp. 8–20, Dec. 2015.

[36] R. Verma, S. Bhattacharya, and S. Mahapatra, "Thermoelectric performance of a single-layer graphene sheet for energy harvesting," *IEEE Trans. Electron Devices*, vol. 60, no. 6, pp. 2064–2070, Jun. 2013.

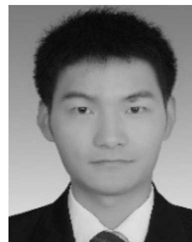

NING WANG was born in 1984. He received the M.S. and Ph.D. degrees in microelectronics from Xidian University, Xi'an, China, in 2009 and 2012, respectively. From 2012, he joined the China North Industries Group Corporation General Electronics Group, Suzhou, China, as a Research and Development Engineer and a Project Leader. From 2013 to 2015, he was a Postdoctoral Researcher with Shanghai Jiao Tong University, Shanghai. Since 2015, he has been a Faculty Member with the University of Shanghai for Science and Technology, Shanghai, where he is currently a Lecturer. His current research interests include high-speed interconnect technology, waveguide in terahertz, and vortex electromagnetic wave.

CONG MENG was born in 1993. She received the Bachelor of Engineering degree in optoelectronic information engineering from the University of Shanghai for Science and Technology, Shanghai, China, where she is currently pursuing the Master of Engineering degree in optical engineering. Her research interest includes thermoelectric cooling.

ZHI-HAO MA was born in 1995. He received the bachelor's degree in optical engineering from West Anhui University, Luan, Anhui, in 2016. He is currently pursuing the Master of Engineering degree with the University of Shanghai for Science and Technology. He is committed to research on the thermoelectric characteristics of graphene.

CONG GAO was born in 1994. He received the bachelor's degree in microelectronics from China Jiliang University, Hangzhou, Zhejiang. He is currently pursuing the Master of Engineering degree in optical engineering with the University of Shanghai for Science and Technology. His research interest includes thermoelectric energy harvesting.

HONG-ZHI JIA was born in 1968. He received the B.S. degree in microelectronics from the Beijing Institute of Technology, Beijing, China, in 1990, and the Ph.D. degree from Xi'an Optical Precision Machinery Research Institute of Chinese Academy of Sciences, Xi'an, China, in 2000. Since 2002, he has been a Faculty Member with the University of Shanghai for Science and Technology, Shanghai, where he is currently a Professor. His current research interests include fiber optical sensors and photodetector.

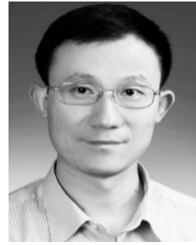

GUO-RONG SUI was born in 1974. He received the Ph.D. degree in optical engineering from the University of Shanghai for Science and Technology, Shanghai, China, in 2008. Since 2008, he has been a Faculty Member with the University of Shanghai for Science and Technology, Shanghai, where he is currently an Associate Professor. His current research interests include high-speed semiconductor device, integrated optics device, and optical-electrical detection.

XIU-MIN GAO was born in 1978. He received the Ph.D. degree from the Shanghai Institute of Optics and Fine Mechanics (SIOM), in 2006, and joined the University of Shanghai for Science and Technology (USST), in 2017. He is currently a Leader of several research programs, including National Natural Science Foundation of China, National Key Research and Development Plan. He has published more than 60 articles in journals, such as *Nature Communications, Scientific Reports*, and *Applied Optics*. He obtained more than 50 patents, and his several research achievements have been industrialized. His current research interests include instruments and meters, smart sensing technology, optical engineering, and precision measurement.